







than  $\tau_B$ , so that the induced  $\overline{v\delta n}$  could be even smaller for transient SBS process with pump or Stokes pulse shorter than  $\tau_B$ .

### 3. Principle and experimental setup

In our scheme, illustrated in Fig. 1, a Brillouin grating is generated by two pump pulses. The frequency of pump 1 is higher than that of pump 2 by a  $\Omega_B$  of optical fiber, and the Brillouin grating has the same motion direction as pump 1. The effective length of the Brillouin grating is  $L_B = (t_{p1} + t_{p2})c/4n$ . In experiment,  $t_{p2}$  is fixed at 2 ns and  $t_{p1}$  is increased from 2 ns to 6 ns to increase the effective length of the Brillouin grating from 0.2 m to 0.4 m. Two pump pulses are launched into the slow axis of PMF, and the probe pulse immediately following pump 2 pulse (the leading edge of probe pulse overlapping with trailing edge of pump 2 pulse) is launched into the fast axis to read the Brillouin grating. Because the probe pulse counter-propagates with the Brillouin grating, coherent anti-Stokes Brillouin scattering (CABS) could occur when the probe pulse interacts with the Brillouin grating, and consequently the scattered light frequency is higher than that of probe pulse by a  $\Omega_B$ . The CABS will be maximized when the frequency difference  $\Delta\nu_{Bire}$  between pump 2 and the probe satisfies the phase-matching condition [11,12].

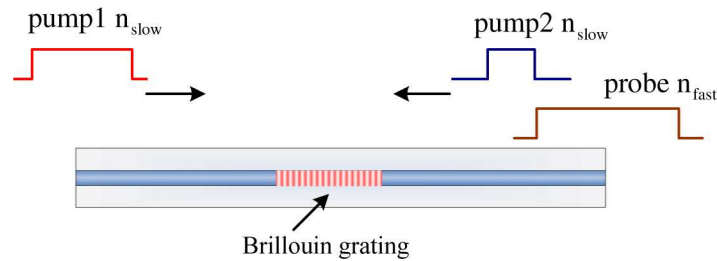


Fig. 1. Schematic diagram of Brillouin grating generation and reading.

The experimental setup is shown in Fig. 2. Two narrow linewidth (3 kHz) fiber lasers operating at 1550 nm are used to provide the pump1 and pump2, respectively, and their frequency difference is locked by a frequency counter. A tunable laser with a wavelength resolution of 0.1 pm is used as probe wave. The frequency difference between pump1 and probe is monitored and recorded by a high-speed detector with a bandwidth of 45 GHz and a 44 GHz electrical spectrum analyzer. Three high extinction-ratio (ER) electro-optic modulators (> 45 dB) are used to generate pump 1, pump 2 and probe pulses. The power of pump 1 pulse, pump 2 pulse and probe pulse in the PMF are about 0.4W, 30 W and 30 W, respectively. A tunable fiber Bragg grating with a bandwidth of 0.2 nm is used to filter out the transmitted pump1 pulse.

A Panda fiber is used in experiment, whose nominal beat-length is smaller than 5 mm at 1550 nm with a BFS of 10.871 GHz at room temperature.

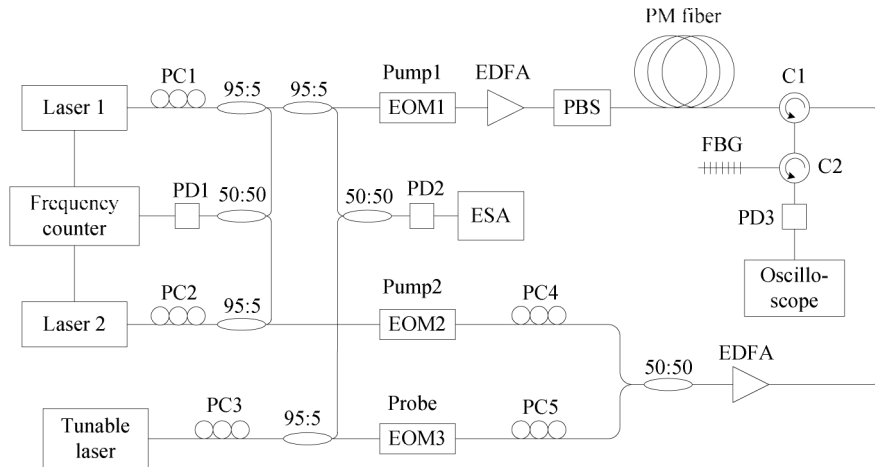


Fig. 2. Experimental setup. PC: polarization controller, EOM: electro-optic modulator, PBS: polarization beam splitter, C: circulator, PD: photo-detector, EDFA: Erbium-doped fiber amplifier, ESA: electrical spectrum analyzer, FBG: fiber Bragg grating.

#### 4. Results and discussions

In Ref. 11, a two-peak structure Brillouin grating spectra were obtained, which was mistakenly explained to be the fine structure of the optical mode. In this paper, we found that the two-peak spectra were induced by the leakage of pump 1 pulse. In experiment, the pump 1, pump 2 and probe pulses were set to 2 ns, 2 ns and 6 ns, respectively. The comparison of measured Brillouin grating spectra with different ER of pump 1 pulse is shown in Fig. 3. The leakage of pump 1 pulse decreases the power of the reflected probe pulse especially when the frequency offset between the probe wave and the pump wave satisfies the phase matching condition, which decreases the intensity of the spectrum and causes a dip at the center of the spectrum resulting in a two-peak structure. The impact of the leakage can be removed by using high ER modulators, and a one-peak spectrum can be obtained as shown in Fig. 3.

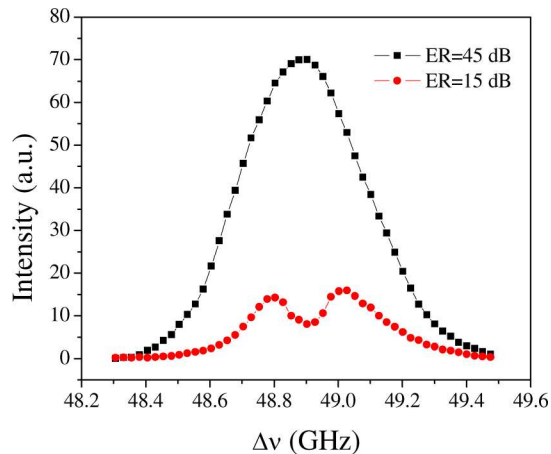


Fig. 3. Measured Brillouin grating spectra with different ER (45 dB and 15 dB) of pump 1 pulse.

Then we investigated the Brillouin grating spectra with different grating lengths.  $t_{p2}$  was fixed at 2 ns and  $t_{p1}$  was increased from 2 ns to 6 ns to increase the effective length of the Brillouin grating from 0.2 m to 0.4 m. The probe pulse width of 6 ns and 8 ns were chosen to read the Brillouin grating, and the measured Brillouin grating spectra are shown in Fig. 4. For

the case of 2 ns pump 1 pulse and 2 ns pump 2 pulse, the effective length of the generated Brillouin grating is 0.2 m and the measured spectra are shown in Fig. 4(a), which fit well with a Gaussian profile. The intensity of the acoustic wave is determined by the interaction time of the pump and the Stokes waves, and thus the generated Brillouin grating is a nonuniform-grating with  $\delta n$  maximizing at the center and decreasing toward two sides. This nonuniform apodization of Brillouin grating results in a Gaussian spectrum without side lobes, which are expected in a uniform-grating [14].

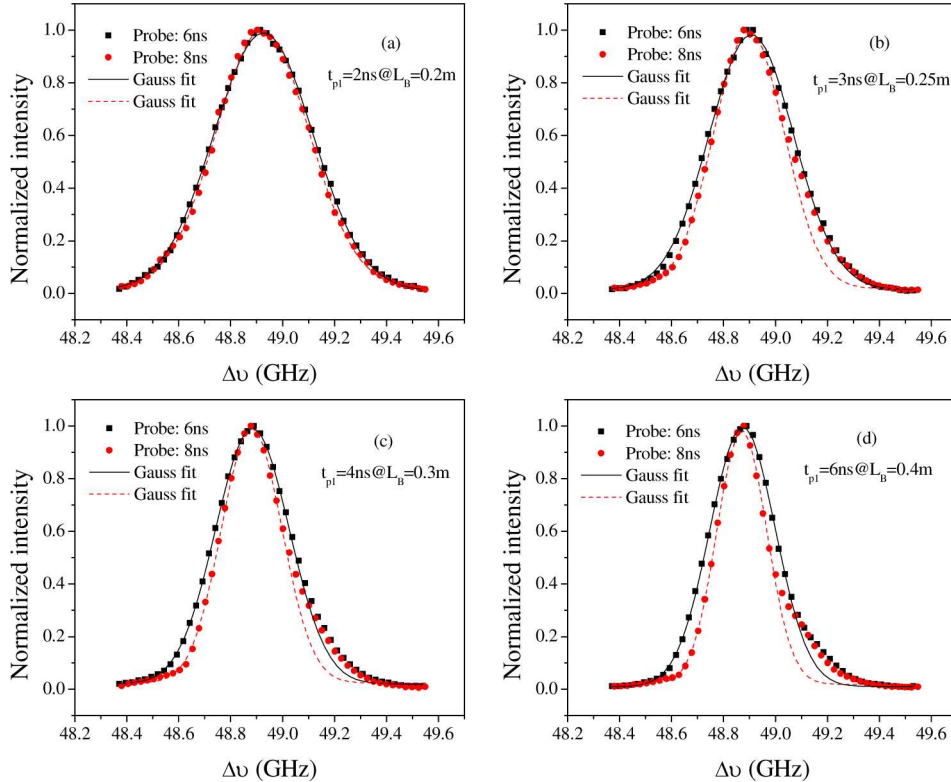


Fig. 4. Measured Brillouin grating spectra with 6 ns and 8 ns probe pulse with different pump 1 pulse width (a) 2 ns, (b) 3 ns, (c) 4 ns, (d) 6 ns. Pump 2 pulse width is constant at 2 ns.

The measured spectrum is the convolution of the probe pulse spectrum and the intrinsic Brillouin grating spectrum, which has been pointed out in previous works [6,17]. The intrinsic Brillouin grating spectrum can be obtained from deconvoluting the probe pulse spectrum out of the measured spectra, and the spectral widths (FWHM) are plotted in Fig. 5. The black curve shows the FWHM spectrum width of weak fiber Bragg grating described by Eq. (4). For 8 ns probe pulse, the measured spectral widths agree very well with the theory of weak fiber Bragg grating; for 6 ns probe pulse, the experimental results also agree with the theoretical curve when the grating length is shorter than 0.3 m, while the discrepancy from the theory at 0.4 m originates from the effective reading-length of the 6 ns probe pulses. These results directly prove that the moving Brillouin grating and the static fiber Bragg grating follow the same basic theory.

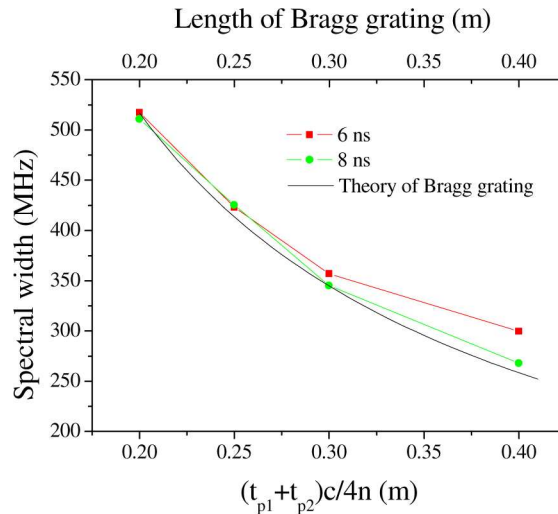


Fig. 5. The intrinsic Brillouin grating spectral width as a function of length.

The other important characteristic of the Brillouin grating is the acoustic wave relaxation or grating decay. The Brillouin grating is created through electrostriction effect and can only be sustained by keeping the two pump waves. After removing the pump waves, the Brillouin grating will exponentially decay, which characterizes an intrinsic Lorentzian Brillouin gain spectrum [15]. In our scheme as shown in Fig. 1, pump 2 pulse is fixed at 2 ns and pump 1 pulse width is increased to prolong the grating length. The Brillouin grating is generated following pump 2 pulse from the right end to the left end, and the intensity of the whole Brillouin grating exhibit a slope due to the acoustic wave decay. For the probe pulse immediately following pump 2 pulse, the front of the probe pulse always read the strongest part of the grating, while the rear of the probe pulse always read the decayed part, which causes the asymmetry of the spectra especially for long gratings as shown in Fig. 4. It is clearly seen that for long gratings the low-frequency side still agrees well with Gaussian profile, while the high-frequency side has a discrepancy and shows a Lorentzian-like wing, which comes from the apodization of the Brillouin grating induced by acoustic wave decay.

To further demonstrate the effect of the apodization of the Brillouin grating induced by the acoustic wave decay, we switched the pulse width of pump 1 and pump 2 pulses with probe pulse still immediately following pump 2 pulse. Figure 6 shows the measured Brillouin grating spectrum with 2 ns pump 1 pulse, 10 ns pump 2 pulse and 6 ns probe pulse. In this case, the Brillouin grating is created following pump 1 pulse from the left end to the right end, and both of the front and the rear of the probe pulse read the decayed grating. We see that the measured spectrum agrees with a Lorentzian profile, which indicates that the acoustic wave decay play an important role in this case. For the case of 2 ns pump 1 and 2 ns pump 2, it is a transient process, where the interaction duration is much smaller than the phonon lifetime, and consequently the grating decay can be neglected, so that the spectra have a Gaussian profile as shown in Fig. 4(a).

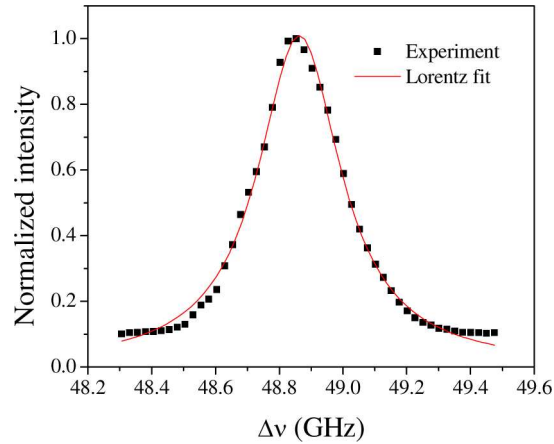


Fig. 6. Measured Brillouin grating spectrum with 2 ns pump 1 pulse, 10 ns pump 2 pulse and 6 ns probe pulse.

In addition, pump depletion can also cause Brillouin grating apodization. In our case, pump 1 and pump 2 correspond to the pump wave and Stokes wave in the SBS process. Because of short interaction duration (2 ns), only a small fraction of power is transferred from pump 1 to pump 2, so that the pump depletion can be negligible when a Brillouin grating is generated.

## 5. Conclusion

In summary, we have investigated the characteristics of the Brillouin grating spectra. First, the criteria of the weak Brillouin grating is analyzed and the calculations show that the Brillouin grating generated in our experiment are in the regime of weak grating. Then we experimentally demonstrated that the Brillouin grating spectrum agrees with the fiber Bragg grating theory but not determined by the natural Brillouin gain bandwidth as thought previously. The apodization of the Brillouin grating induced by the acoustic wave decay were also observed, and both Gaussian and Lorentzian spectra can be obtained depending on the effect of acoustic wave decay. Compared with the fixed fiber Bragg grating, the Brillouin grating can be conveniently created at arbitrary position with variable length, which can be used as a position- and bandwidth-adjustable filter in sensing, optical communication and other applications.

## Acknowledgments

The authors would like to thank Natural Science and Engineering Research Council of Canada (NSERC) Discovery Grants and Canada Research Chair program for the financial support of this research.